Water Resources Research

RESEARCH ARTICLE
10.1029/2023WR036942

Estimating Daily Snow Density Through a Spatiotemporal Random Forest Model

Liyang Sun[1], Xueliang Zhang[1], Huadong Wang[1], Pengfeng Xiao[1,2,3], and Yunhan Wang[1]

[1]Jiangsu Provincial Key Laboratory of Geographic Information Science and Technology, Key Laboratory for Land Satellite Remote Sensing Applications of Ministry of Natural Resources, School of Geography and Ocean Science, Nanjing University, Nanjing, China, [2]Frontiers Science Center for Critical Earth Material Cycling, Nanjing University, Nanjing, China, [3]Jiangsu Center for Collaborative Innovation in Geographical Information Resource Development and Application, Nanjing, China

Key Points:

- A spatiotemporal random forest (STRF) model is proposed for estimating large-scale and long-term snow density
- STRF depicts the spatiotemporal dependent structure of snow density and handles its nonlinear relations with various influencing factors
- The estimated snow density outperforms ERA5-Land snow density and could improve snow water equivalent data set using fixed snow density

Correspondence to:
X. Zhang,
zxl@nju.edu.cn

Citation:
Sun, L., Zhang, X., Wang, H., Xiao, P., & Wang, Y. (2024). Estimating daily snow density through a spatiotemporal random forest model. *Water Resources Research*, *60*, e2023WR036942. https://doi.org/10.1029/2023WR036942

Received 18 DEC 2023
Accepted 17 JUL 2024

Author Contributions:
Conceptualization: Xueliang Zhang
Data curation: Liyang Sun, Xueliang Zhang
Methodology: Liyang Sun, Huadong Wang
Supervision: Xueliang Zhang
Validation: Liyang Sun
Writing – original draft: Liyang Sun
Writing – review & editing: Xueliang Zhang, Huadong Wang, Pengfeng Xiao, Yunhan Wang

Abstract Snow density is of paramount importance in water resource management, snow avalanche warning, and climate change research. However, the lack of competent methods for long-term and vast-scale snow density mapping persists due to the intricate spatiotemporal dependencies inherent in snow density, resulting in scarce and inaccurate snow density products. To address this challenge, a spatiotemporal random forest (STRF) model is constructed by leveraging in-situ measurements, multisource remote sensing, and reanalysis data. It tackles the spatiotemporal dependencies in snow density arising from its inherent heterogeneity and the relations involving snow density and nonlinearly connected meteorological, terrain, vegetation, and snow-related factors. The effectiveness of the model is substantiated through rigorous validation methods, including random, temporal, and spatial block cross-validations as well as independent validation, apparently surpassing ERA5-Land snow density. The estimated snow density is also demonstrated to be able to improve existing snow water equivalent data set using fixed snow density. Utilizing the proposed model, a data set of daily 25-km snow density from 1980 to 2018 is constructed for stable snow cover areas in China, which holds significant potential for research and applications in the realm of snow hydrology.

Plain Language Summary Snow density plays a crucial role in managing water resources and issuing snow avalanche warnings. Snow density exhibits great spatiotemporal dependent structure due to its spatiotemporal heterogeneity and its relations with various influencing factors, which pose challenges to mapping long-term and large-scale snow density. This leads to a scarcity of accurate snow density products. To tackle this issue, we develope a spatiotemporal random forest (STRF) model by combining ground measurements, remote sensing sources, and reanalysis data. Notably, our model shows impressive results apparently outperforming the ERA5-Land snow density data set. Our estimated snow density can also enhance existing snow water equivalent data set that rely on fixed snow density. Using our model, we produce a data set of daily 25-km snow density from 1980 to 2018 for stable snow cover areas in China. This data set holds significant potential for research and practical applications in the field of snow hydrology.

1. Introduction

Snow density serves as a pivotal parameter in the snowpack, impacting its thermal, mechanical, and optical characteristics. It plays a prominent role in substantial snow-related studies and applications, such as water resource management, snow avalanche warning, and weather and climate forecasting (Wang et al., 2023). Snow density exhibits morbid spatiotemporal heterogeneity, which manifests across various stages of snow evolution (McCreight & Small, 2014; Yang et al., 2019). However, in many snow-related studied and applications, snow density is often treated as a fixed value due to limited knowledge about its distribution, especially for snow water equivalent (SWE) estimation, which highly influences the accuracy of SWE products obtained through passive microwave remote sensing (Yang, Jiang & Lemmetyinen et al., 2020; Yang, Jiang & Luojus et al., 2020; Zaremehrjardy et al., 2021). A recent study revealed that dynamic snow density obtained by simple interpolation techniques could improve the accuracy of SWE products by 16% (Venäläinen et al., 2023). Accordingly, a comprehensive understanding of dynamics snow density is urgent for advancing insights into hydrological processes (Gao, Li, Zhang & Chen et al., 2022; Gao, Li, Zhang & Zeng et al., 2022).

Ground station observations are considered as the most convenient and accurate method for obtaining snow density, and are frequently utilized to investigate the spatiotemporal distribution of snow density (Hao

et al., 2021). However, these ground observations usually succumb to scarce and unbalanced station distributions, rendering it impractical to obtain large-scale spatiotemporal snow density data. An alternative approach involves deriving consecutive snow density using physical models, such as SNOWPACK (Lehning et al., 2002), Crocus (Durand et al., 1999), and $\Delta SNOW$ (Fontrodona-Bach et al., 2023). These models can effectively simulate diverse snow variables including snow density. However, due to their high complexity and the need for a large volume of atmospheric forcing, these models become time-consuming and computationally expensive when applied to vast-scale snow density mapping (Raleigh & Small, 2017).

Other studies usually invert snow density based on microwave remote sensing. For example, Li et al. (2022) inverted dry snow density based on C-band synthetic aperture radar data ($R = 0.868$), which considers both snow ground interface scattering and volume scattering. Gao et al. (2023) employed Soil Moisture Ocean Salinity satellite radiometer observations and considered the forest influence to estimate snow density. However, despite these efforts, there are currently no available snow density products derived from remote sensing measurements owing to the multiparameter morbid inversion problem (Gao, Li, Zhang & Chen et al., 2022; Gao, Li, Zhang & Zeng et al., 2022). Besides, current studies usually use statistical models to estimate snow density by incorporating climatic and snow-related variables, such as linear regression model (Valt et al., 2018), Bayesian model (Bruland et al., 2015; Sturm et al., 2010), and artificial neural network model (Broxton et al., 2019). Despite the potential for these statistical models to extrapolate snow density, their accuracy has proven unsatisfactory due to the neglect of spatiotemporal dependent structure inherent in snow density.

The spatiotemporal dependent structure inherent in snow density encompasses its spatiotemporal heterogeneity and its relations with influencing factors. Snow density is sensitive to temporal variation owing to climatic variation (Jonas et al., 2009; Svoma, 2011), and has abundant spatial variation caused by the interaction with variables, such as topography, land cover, radiation, and wind (Elder et al., 1998; Grünewald et al., 2010). Moreover, snow density and its influencing factors exhibit complex relations that display spatiotemporal heterogeneity and are hardly stationary (Dai & Che, 2011). These spatiotemporal heterogeneities in snow density and their relations with influencing factors collectively create the spatiotemporal dependent structure inherent in snow density. It is essential to carefully consider this structure in statistical models to avoid violating the assumption of independence and the potential for overfitting, especially for extrapolations (Roberts et al., 2017). Although spatiotemporal interpolation methods hold the potential to depict spatiotemporal heterogeneity of snow density, such as kriging interpolation and inverse distance interpolation (Goovaerts, 1997; Shepard, 1968), they are unable to figure out the nonlinear relations between snow density and influencing factors. In addition, since the observed values are involved in inference, interpolation methods fail to achieve long-term mapping when the temporal range of the observed samples is limited.

The typical statistical solution to address this problem involves applying suitable parametric models that explain the respective dependent structure, such as spatial or temporal autoregressive models and phylogenetic least squared regression. For example, Wang et al. (2023) made progress in mapping snow density by considering the spatiotemporal dependent structure inherent in snow density based on the geographically and temporally weighted neural network (GTWNN). However, the GTWNN model is an interpolation model, which achieves inferencing unobserved snow density by exploring the spatiotemporal similarity between the unobserved site and its nearby observed samples. Hence, the observed samples are directly involved in the inference process. This leads to two defects: (a) the inference performance would highly depend on the distribution of observed samples, where the sparse distribution would result in inferior inference performance; (b) the GTWNN model is not able to achieve snow density inference when there are no observed samples, where the GTWNN model can only obtain snow density maps from 2013 to 2018 in China because of the limited observation conditions, and snow density maps outside these years could not be obtained by GTWNN model.

Current approaches are limited by complexity or structural problems as well as challenges from the spatiotemporal dependent structure inherent in snow density, which leads to rare and unsatisfactory performance of snow density data. The only three available reanalysis snow density data sets are provided by the European Center for Medium-Range Weather Forecasts (ECMWF) Integrated Forecasting System, including European Reanalysis (ERA)-Interim, ERA5, and ERA5-Land, which have varying degrees of estimation errors in China (Gao, Li, Zhang & Chen et al., 2022; Gao, Li, Zhang & Zeng et al., 2022) and hardly meet the needs of hydrological applications.

In this study, we aim to establish a spatiotemporal model capable of producing extensive and long-term snow density maps by capturing the complex relations between snow density and its various influencing factors. The ensemble learning approach Random Forests (RF) (Breiman, 2001) with strong adaptability and nonlinear processing capacity even in multi-collinearity situations is introduced to spatiotemporally extrapolate snow density. In addition, diverse spatiotemporal covariates derived from influencing factors and spatiotemporal information are imbedded in the model to address the spatiotemporal dependent structure inherent in snow density. The main objectives are (a) to construct an RF model for estimating dynamic snow density by handling the nonlinear relations derived from snow density with its influencing factors, (b) to propose effective spatiotemporal covariates for characterizing the spatiotemporal dependent structure inherent in snow density, and (c) to derive daily snow density product from 1980 to 2018 using the proposed model to better assess the spatiotemporal patterns of snow density across China.

2. Materials and Methods

2.1. Ground Observation

Snow shows strong spatiotemporal heterogeneity in China, with abundant snow concentrated in three stable snow cover areas, including Xinjiang (XJ), Northeast-Inner Mongolia (NIM), and the Qinghai-Tibetan Plateau (QTP) snow cover areas (Huang et al., 2016). The three areas cover 27% of the snow cover areas of the country in winter, according to the multiyear average data. The snow cover over the three areas is located on different land cover types and has unique climatology distinguished from each other, which leads to distinct snow characteristics and therefore poses R^2 a great challenge to snow density estimation.

NIM has diverse and uneven land cover types, where forest, grassland, and cropland are dominant. Forest coverage accounts for 40% of NIM and often has relatively deep snow, which is a large source of uncertainty for snow variable estimation (Che et al., 2016). The southern and northern parts of XJ are mainly grassland, while the central part is mainly desert, baer land, and mountains (Ran et al., 2012). Relatively thick snow cover and complex mountains are mainly distributed in northern XJ with the highest annual average snow depth among the three stable snow cover areas (Huang et al., 2019; Yang, Jiang & Luojus et al., 2020; Yang, Jiang & Lemmetyinen et al., 2020). QTP is characterized by complex terrain with an average elevation above 4,000 m and a relatively minimum annual snow depth of approximately 5 cm (Dai et al., 2018). The spatial distribution of snow cover in QTP highly depends upon the complicated terrains and available moisture sources (Pu et al., 2007; Pu & Xu, 2009).

Daily ground snow depth and snow pressure observations of 233 stations from China Meteorological Administration are gathered to calculate snow density (g/cm^3) and SWE (mm) (Figure 1). These observations span three stable snow cover areas and cover the period from 2013 to 2018. A total of 12,868 ground snow density samples are collected to train and validate the proposed model, in which 90% samples from 47.5% stations and the sample numbers of 43% stations are lower than 20, indicating the high spatial heterogeneity of station distribution and challenge for spatial modeling. In addition, a total of 474 samples from 147 snow pits of snow measurement route and 10 snow stations from 2017 to 2018 are used for independent validation, which are collected from the National Cryosphere Desert Data Center (http://www.ncdc.ac.cn/portal/). Given that the intensive ground observations primarily occur from September to May of the next year (snow season), we concentrate on snow density estimation during the snow season.

2.2. Remote Sensing and Reanalysis Data

Multisource remote sensing and reanalysis data are used to calculate five categories of features incorporated into the model, accounting for the spatiotemporal structure in snow density, for a total of 36 features, as shown in Table 1. The selection of each category of input features is informed by insights from previous studies and the specific reasons for employing these features are elucidated as follows.

The snow-related features encompass snow depth, snow cover duration (SCD), snow cover onset date (SCOD), snow cover end date (SCED), snow cover extent (SCE), snow density (SDE), temperature of snow layer (TSL), accumulated snowmelt (SM) and snowfall (SF), sourced from three data sources. Snow density tends to increase with snow age and snow depth, driven by the processes of metamorphism and compaction (Bormann et al., 2013). The passive microware remote sensing snow depth data (CSWE) (Jiang et al., 2022) is consequently used as a key

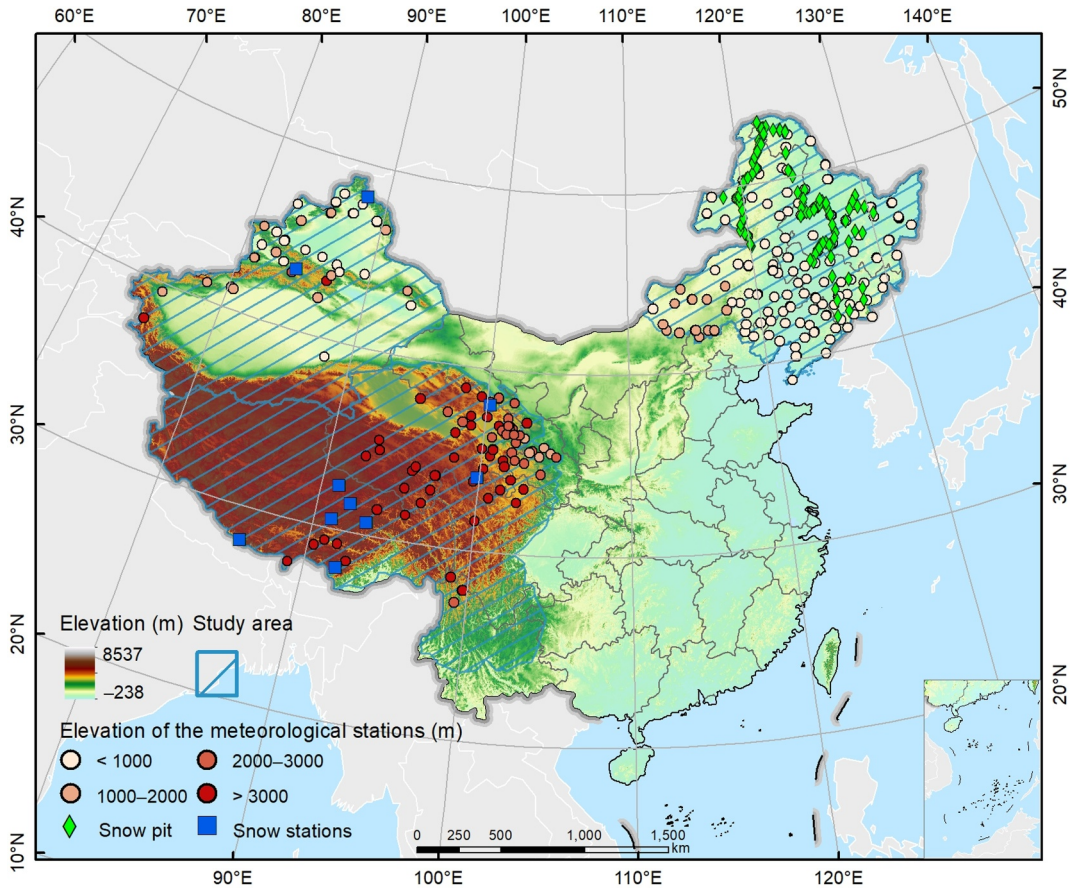

Figure 1. Meteorological stations, snow pits, and snow stations in the stable snow cover areas of China.

variable for estimating snow density. The SCOD, SCED, and SCD are computed from Advanced Very High Resolution Radiometer (AVHRR) SCE data (Hao et al., 2021; Wang et al., 2022). These features account for the effect of snow duration, with SCE reflecting the basic distribution of snow. Additionally, SDE, snowmelt, snowfall, and TSL are extracted from ERA5-Land data set (Muñoz-Sabater et al., 2021), which is the fifth product generated by the ECMWF to provide consecutive land variables. Among three available snow density products, ERA5-Land snow density has been validated to be relatively more effective (Gao, Li, Zhang & Chen et al., 2022; Gao, Li, Zhang & Zeng et al., 2022) and is thus used to provide the basic spatiotemporal patterns of snow density for estimation. TSL is a critical factor to indicate snowmelt. According to daily snowmelt and snowfall data, SF and SM are calculated to represent the effect of snow accumulation and snowmelt.

Table 1
Summary of the Input Features for the Model

Category	Source	Feature	Number
Snow-related	CSWE	Snow depth	9
	AVHRR SCE	SCD, SCOD, SCED, and SCE	
	ERA5-Land	SDE, TSL, SF, and SM	
Meteorology	CMFD	Temp, Prec, RH, WS, SP, Srad, and Lrad	7
Vegetation	ERA5-Land	HVI and LVI	2
Time		DOY and Snow-DOY (D1, D2)	3
Geo-space	DEM	Geo-space distance (*North*, *East*, *West*, *South*, and *Center*)	15
		Mean and standard deviation of topological features (elevation, slope, aspect, PC, and TPI)	

Meteorological features, including wind speed (WS), air temperature (2-m) (Temp), relative humidity (RH), precipitation (Prec), surface pressure (SP), downward shortwave radiation (Srad), and uplink longwave radiation (Lrad), are involved in the model. These features are sourced from China Regional Surface Meteorological Element Driven Data set (CMFD) (He et al., 2020). They serve to denote the environment of falling snow and radiation receiving and generally determine the fresh snow density and snow evolution process.

The vegetation data (leaf area index of high vegetation (HVI) and that of low vegetation (LVI)) come from ERA5-Land data set. HVI and LVI play a crucial role in understanding the impact of surface type. Surface types are of significance to snow density estimation due to its effects of mass, delivery, wind, and radiation (Bonner et al., 2022; Clark et al., 2011). The mass effect caused by canopy interception loss leads to a decrease in the amount of snow, typically resulting in low densification rates and low-density snow (Storck et al., 2002). The delivery effect denotes the process that snow or snowmelt is trapped and delivered to the underlying snowpack (Winstral & Marks, 2014). The wind effect arises from wind packing, which refers to the reduction of wind speed caused by forest impediment and bring about a higher snow density than open space. The radiation effect can change snow density by dominating snow layer temperature and freeze-thaw cycles (Essery et al., 2008). The diverse surface types result in different effects of mass, delivery, wind, and radiation.

Considering that snow density exhibits intense temporal heterogeneity and snow-season cycle, the temporal features in our model include not only the day of the year (DOY) but also Snow-DOY. As snow is considered as a three-phase substance constituting ice, liquid water, and air, snow season usually is divided into snow accumulation and snowmelt periods. The accumulation period contains the processes of compaction and metamorphism, which characterizes the interaction of snowfalls and typically indicates low liquid water and low snow density. The snowmelt period consists of warming, ripening, and output processes, often manifested by higher liquid water and higher snow density (Colombo et al., 2023). These temporal characteristics of snow density have apparent similarity in every snow season, Snow-DOY is thus proposed to depict snow-season cycle, which includes D1 and D2 obtained by calculating the temporal distances from a certain day to SCOD and SCED, respectively, as shown in Equations 1 and 2.

$$\mathrm{D1} = |\mathrm{SCOD} - \mathrm{DOY}| \tag{1}$$

$$\mathrm{D2} = |\mathrm{SCED} - \mathrm{DOY}| \tag{2}$$

Generally, as snow density has strong spatial heterogeneity, the geo-space features including Geo-space distance and fine topological features are adopted to enhance the spatial expression of the model. It has been agreed that snow density increases with latitude and has strong relations with longitude (Zhong et al., 2014, 2021). Different from previous studies that using the simple longitude and latitude with a sudden value change occurs between 180°W and 180°E longitude (Hu et al., 2021), Geo-space distance *North*, *East*, *West*, *South*, and *Center* are incorporated in the RF model to better distinguish spatial differences and consequently express the spatial heterogeneity of snow density. The Geo-space distance denotes the five Haversine distances of one point to the northernmost (*North*), easternmost (*East*), westernmost (*West*), southernmost (*South*), and center (*Center*) of the study area.

The accumulation and melt of snow are heavily influenced by local terrain, which highly affects the distribution of snow density (Sturm & Wagner, 2010; Trujillo et al., 2007). Elevation is used as the key indicator of snow accumulation and melt (Anderton et al., 2004). The aspect, slope, and profile curvature (PC) influence the redistribution and the radiation absorbed of snow (Wetlaufer et al., 2016). Besides, topographic position index (TPI) is used to refer to the height gradient information of a pixel compared to surrounding pixels and thus explains the redistributive impact of wind on snow (Meloche et al., 2022; Revuelto et al., 2014), as shown in Equation 3

$$\mathrm{TPI} = \mathrm{int}(dem - \mathrm{mean}(dem, annulus, irad, orad)) \tag{3}$$

where int refers integer, mean refers average, *irad* refers the inner radius of annulus, and *orad* refers the outer radius of annulus.

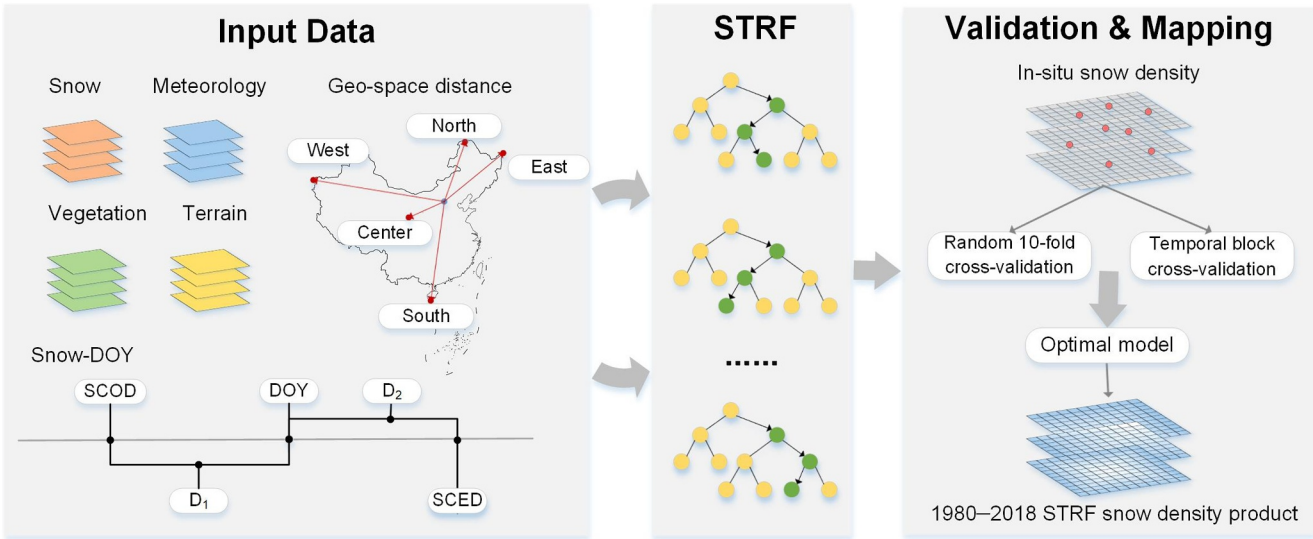

Figure 2. Flowchart summarizing the STRF snow density data estimation, which consists of data input, STRF model, model validation, and snow density mapping.

These topological features are obtained from the Shuttle Radar Topography Mission Digital Elevation Model (DEM) with 90-m resolution. Particularly, we first calculate topological variables at a resolution of 90 m and then compute the mean and standard deviation of each variable within the range of 25 km, to explicitly explain the relief. Regarding data processing, all the gridded data are resampled to the same spatiotemporal resolution (daily, 25 km).

2.3. STRF Model

Random forest (RF) is an ensemble learning technique that utilizes numerous decision trees for supervised classification and regression tasks based on the relations between independent and dependent variables (Breiman, 2001; Prasad et al., 2006). Compared with other regression tree approaches, RF can handle complex nonlinear relations and predict unbiased estimates without overfitting to the training data set, even for small sample sizes (Zhang et al., 2021). Hence, with the advantages of handling strong nonlinear relations and being highly robust, RF is chosen as a suitable model to deal with remote sensing data and high-dimensional feature spaces for snow density estimation. Furthermore, the spatiotemporal features embedded to RF model to construct a spatiotemporal RF (STRF) model without updates in RF machine learning structure. The STRF model can express the spatiotemporal dependent structure inherent in snow density, which is shown in Figure 2.

First, we obtain values of the above-mentioned features as the input data and the in-situ snow density as the target data to train STRF model. Second, the STRF model is trained to obtain the optimal model. There are four parameters to be specified by grid search and cross-validation: (a) the number of employed trees (fixed at 440); (b) the maximum depth of regression trees (fixed at 23); (c) the minimum number of samples to split per node (fixed at 10); and (d) the maximum number of features to build regression trees (max_features) (fixed at 7). The number of features to build trees is usually 1/3 of the total number of variables. Another choice is to set the max_features as sqrt (the number of input features) or log2 (the number of input features) (~7) because low max_features is beneficial for increasing randomness, reducing overfitting, and accelerating training speed. Third, the trained optimal STRF model is employed with gridded covariates to estimate daily snow density for China from 1980 to 2018.

2.4. Validation Method

The K-fold cross-validation strategy, capable of alleviating the problem of overfitting and obtaining a more robust model, is used to train and validate the model. The spatiotemporal patterns of snow density are so complicated that the unbalanced observations in our study are insufficient for encompassing snow density characteristics. To address this, the K-fold cross-validation strategy is used to incorporate more samples in model training. Accordingly, several complimentary validation methods should be used to gain insights from multiple

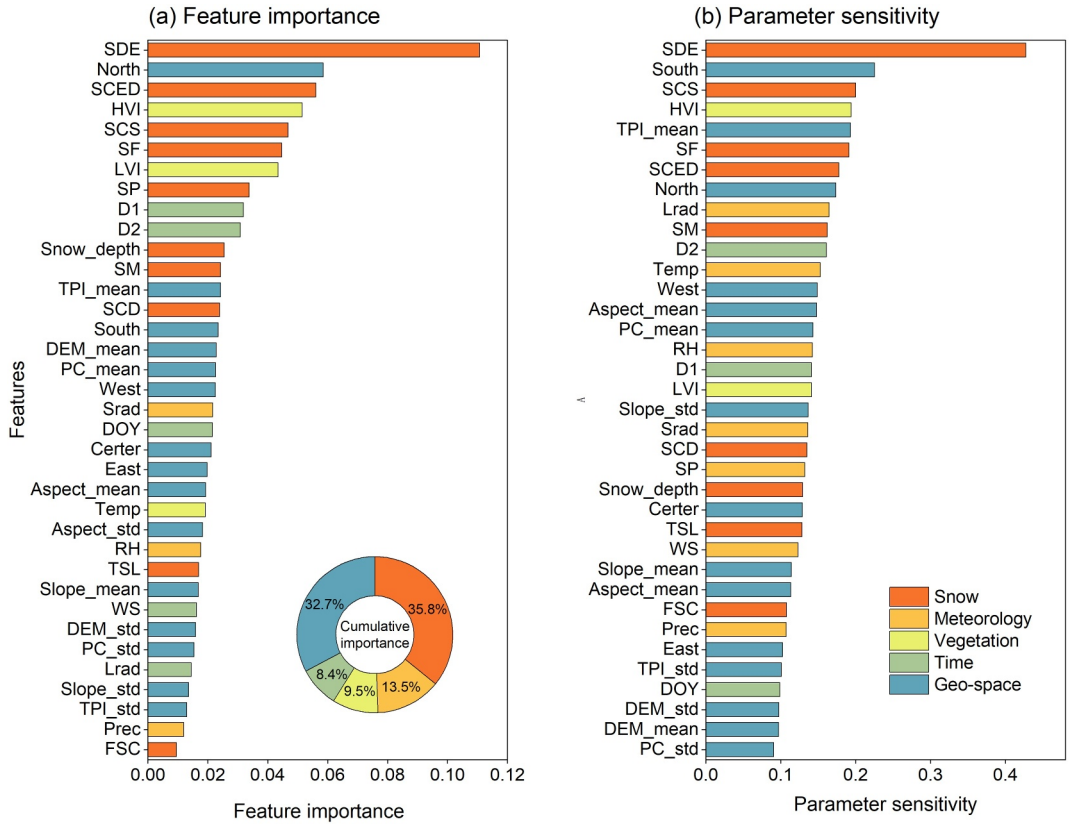

Figure 3. Feature importance (a) and parameter sensitivity (b) of the STRF model.

perspectives due to the difficulty of guaranteeing independence and stationarity in spatial variables (Stock, 2022). Therefore, both random 10-fold cross-validation, temporal block cross-validation, spatial block cross-validation, and independent validation strategies are utilized to fully evaluate the performance of model by using three statistical indicators, including fitting coefficient (R^2), root mean square error (RMSE, g/cm^3), and the mean absolute error (MAE, g/cm^3).

The random 10-fold cross-validation strategy is conducted to randomly divide samples into 10 folds, one for model validation in turn and the others for model fitting based on the principle of K-fold cross-validation technique (Rodriguez et al., 2010). The temporal block cross-validation strategy is equal to 6-folds cross-validation, which divides samples by year, 1 year for model validation in turn and the others for model fitting. The 6 validation results are summarized to evaluate model performance and to provide perspectives on the temporal prediction of the model. It is noted that the temporal block cross-validation could help demonstrate the effectiveness of the estimated snow density from 1980 to 2018 considering that the in-situ observations only cover the years from 2013 to 2018. The spatial block cross-validation strategy divides samples by station and can provide perspectives on the spatial prediction of the model.

3. Results

3.1. Snow Density Estimation Accuracy

3.1.1. Overall Accuracy

The feature analysis is first investigated by feature importance and feature sensitivity to understand the impacts of the covariates on the trained STRF model, as shown in Figure 3. The feature importance is ranked by the mean decrease accuracy, making random forest physically interpretable for model construction (Breiman, 2001).

The snow-related variables are dominant with the highest overall importance of 35.8% (Figure 3a), within which ERA5-Land snow density is the most important because it provides a first guess in snow density for estimation.

Table 2
Model Accuracies Comparison Among Nonlinear and Linear Models

	RF	XGBoost	LGBM	MLR	Bayesian
MAE	0.024	0.025	0.024	0.039	0.038
RMSE	0.036	0.038	0.037	0.056	0.054
R^2	0.642	0.621	0.636	0.178	0.184

The collective importance of spatial covariates and temporal terms accounts for 32.7% and 8.4% of overall importance, respectively, highlighting important roles played by spatiotemporal covariates in the model and emphasizing the necessity of considering the spatiotemporal dependent structure inherent in snow density. Meteorological and vegetation features also play important roles, especially HVI, LVI, and surface pressure.

The parameter sensitivity analysis between snow density and covariates reflects the model's robustness to features and identify the sensitive parameters (Figure 3b). The parameter analysis is based on the extended Fourier amplitude sensitivity test (EFAST) algorithm, which considers the variance of the model input caused by the input parameters and the interaction among the parameters (Gao, Li, Zhang & Chen et al., 2022; Gao, Li, Zhang & Zeng et al., 2022). The ERA5-Land snow density is the primary sensitive factors of 0.427, followed by South, SCS, and HVI.

We evaluated the performance of the commonly used models on the same data and random 10-folds cross-validation strategy to demonstrate the effectiveness of RF in estimating snow density, including extreme gradient boost (XGBoost), light gradient boosting machine (LGBM), linear regression model (MLR), and Bayesian model. The results in Table 2 show that the accuracies of nonlinear models (RF, XGBoost, LGBM) all surpass those of linear models (MLR and Bayesian model), indicating the importance of depicting nonlinear relations between snow density and spatiotemporal variables. Since the strategies of randomly selecting features and sampling with dropout enable RF to handle high-dimensional, redundant features and reduce overfitting, the RF achieves the best performance with R^2 of 0.642, followed by LGBM with R^2 of 0.636.

The estimated snow density from the STRF model is compared to ERA5-Land snow density to further demonstrate its effectiveness. The results show that the STRF snow density attains apparently higher accuracy with an improved regression line (Figure 4). The STRF snow density based on random cross-validation attains the

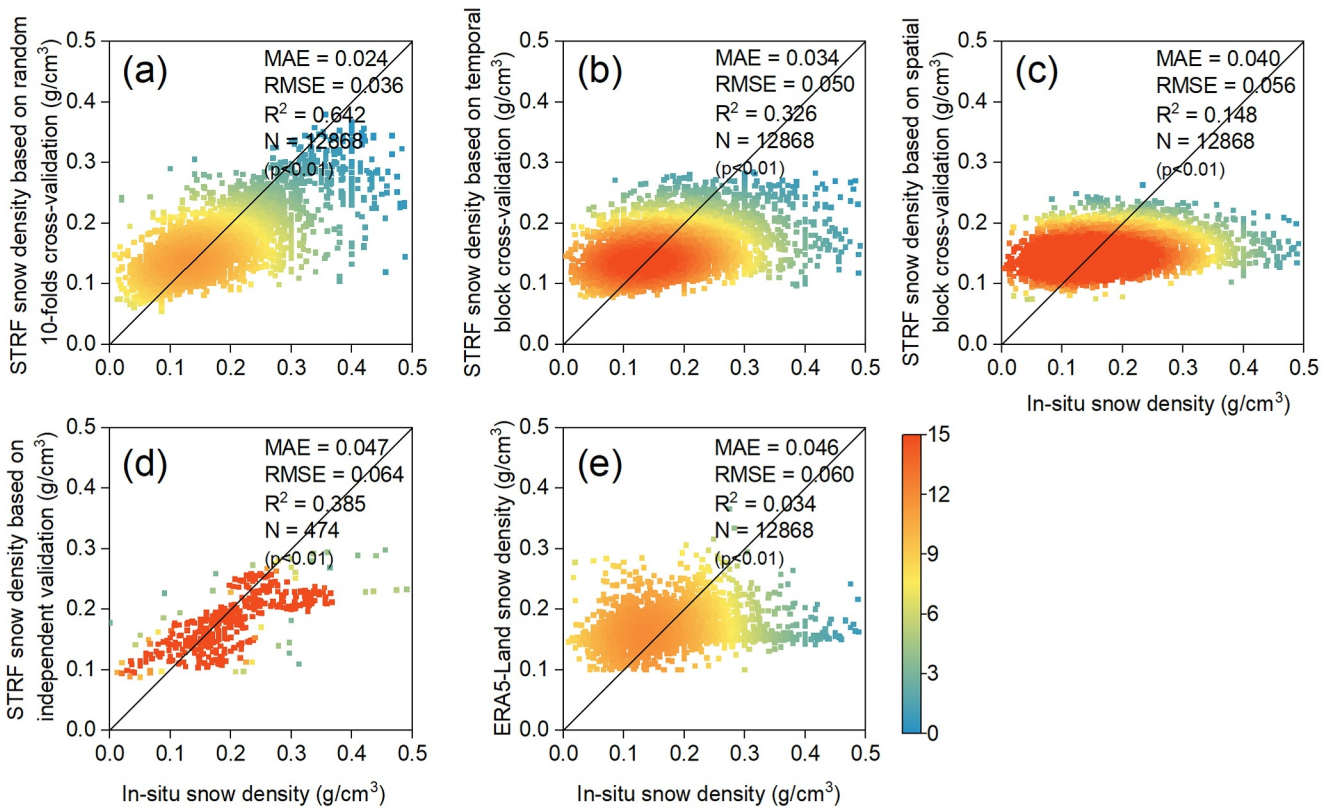

Figure 4. Accuracies of the STRF model indicated by (a) random 10-folds cross-validation and (b) temporal block cross-validation, (c) spatial block cross-validation, (d) independent validation, and (e) the ERA5-Land snow density data.

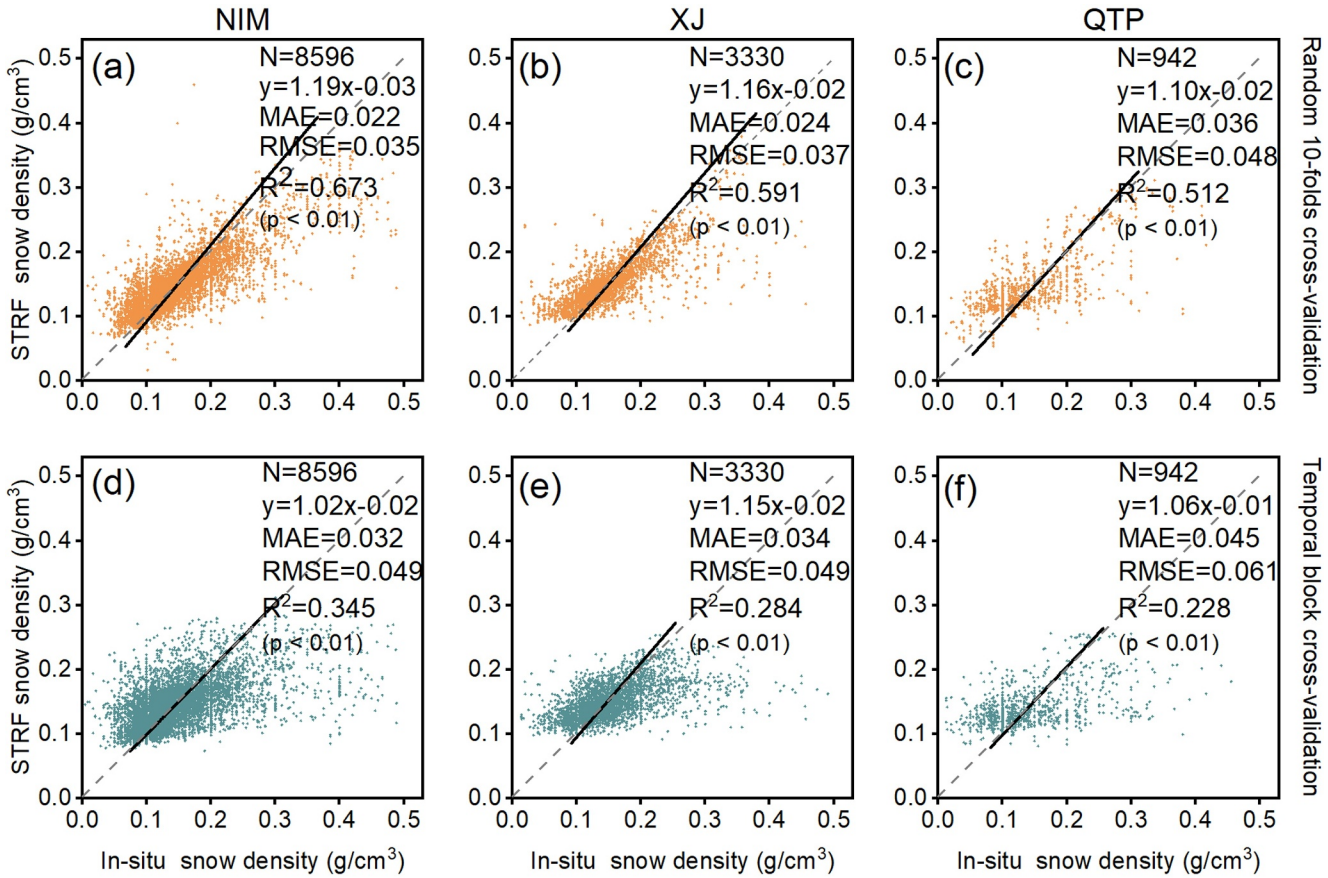

Figure 5. Accuracies of the STRF model based on random 10-folds cross-validation and temporal block cross-validation in three snow cover areas, in which N refers to the number of samples.

highest overall accuracy (R^2 = 0.642, MAE = 0.024 g/cm^3, and RMSE = 0.036 g/cm^3), declaring that 64.2% of daily snow density fluctuations can be explained by STRF model (Figure 4a). The accuracy of STRF snow density based on temporal block cross-validation demonstrates the effectiveness of temporal prediction with an R^2 of 0.326, and the majority of the points are clustered along the trend line with a slope of 1.0 (Figure 4b). The STRF snow density based on spatial cross-validation demonstrates the potential of spatial prediction with an R^2 of 0.148 under imbalanced distribution of observation numbers among the stations (Figure 4c). The accuracy of STRF snow density based on independent validation demonstrates the robustness of STRF model with an R^2 of 0.385 (Figure 4d). The accuracies of temporal and spatial block cross-validation (Figures 4b and 4c) are lower than that of random cross-validation (Figure 4a), which can be attributed to the training samples in temporal/spatial block cross-validation not containing the samples of predicting year/station while the training samples in random cross-validation cover all years/stations. Compared with the ERA5-Land snow density, the accuracy of STRF snow density increases the R^2 from 0.034 to 0.642. These results collectively affirm the effectiveness of the model, as validation results show that STRF model could handle the weak-correlated covariates well and the embedded covariates depict spatiotemporal dependent structure inherent in snow density.

3.1.2. Accuracies at Different Snow Cover Areas

The diverse precipitation and temperature conditions as well as terrain and underlying surface lead to distinguished snow characteristics in different snow cover areas. Therefore, the accuracies of estimated snow density from the STRF model are evaluated at different snow cover areas, including NIM, XJ, and QTP.

Both validation results indicate that the NIM presents the best accuracy, successively followed by the XJ and QTP. The NIM achieves the highest R^2 of 0.673 based on random cross-validation (Figure 5a), with less complex topography and intermediate snow accumulation and the most abundant samples. In XJ, STRF snow density

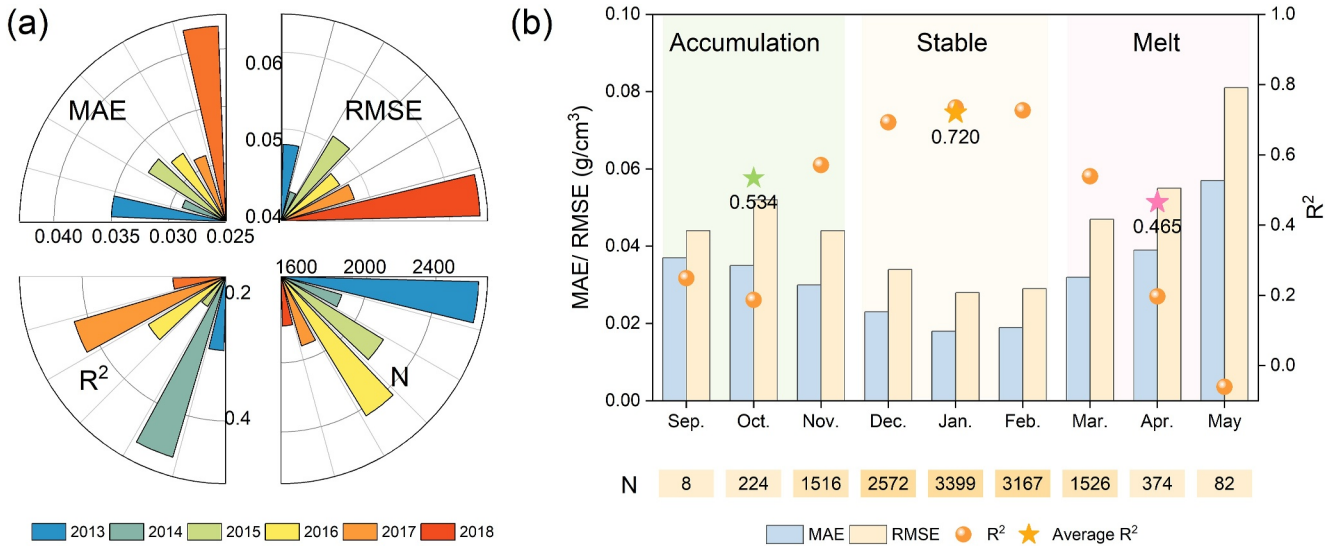

Figure 6. Accuracies of the STRF model at different temporal scales. (a) The yearly accuracy based on temporal block cross-validation, and (b) the accuracy in different seasons and months based on random cross-validation, in which N refers to the number of samples.

presents excellent performance with R^2 of 0.591 and 0.284 with the most snow accumulation and sound samples (Figures 5b and 5e). The QTP has the relatively lower accuracy with R^2 of 0.512 and 0.228 (Figures 5c and 5f), which is mainly because the snow density varies dramatically in the QTP with complicated topology, varied climate regimes, and synoptic forcing. It is noted that there are sparse and uneven stations over the QTP with only 943 samples, partly leading to the limited regional representativeness of observations in the QTP.

3.1.3. Accuracies at Different Temporal Scales

The temporal block cross-validation accuracies in different years are evaluated to reveal the temporal prediction ability of STRF model (Figure 6a). In general, daily snow density estimates derived from STRF model agree well with in-situ snow density measurements among different years (R^2 = 0.226–0.470, MAE = 0.029–0.042 g/cm^3, and RMSE = 0.041–0.064 g/cm^3). The fluctuating performance of STRF model in different years is partly attributed to the varied data volume and snow conditions.

The random cross-validation accuracies at seasonal and monthly scales are determined to present the difference of model performance within a year (Figure 6b). The snow season is categorized into three periods considering the characteristics of snow season (Ke et al., 2016): snow accumulation period (Sep.–Nov.), the snow stable period (Dec.–Feb. of the next year), and the snowmelt period (Mar.–May). At seasonal scale, the STRF snow density shows the highest accuracy during the snow stable period, reaching an R^2 of 0.720, in which January has the highest R^2 of 0.735, the lowest MAE of 0.018 g/cm^3, and RMSE of 0.028 g/cm^3. This is because snow state remains stable and relatively adequate observations during the snow stable period. Contrary to snow stable period, the other two periods have relatively rapid changes in snow, more observation errors, and fewer observations, resulting in inferior model performance, particularly in the months of October, April, and May.

3.1.4. Optimizing SWE Products With Estimated Snow Density

One of the critical purposes of producing dynamic snow density data is to improve SWE products with a fixed snow density. Therefore, the comparisons between original SWE product and optimized SWE with dynamic snow density (STRF and ERA5-Land snow density) are conducted to further demonstrate the effectiveness of STRF model. We select CSWE and GlobSnow SWE products because they have higher accuracies and spatiotemporal continuity according to the evaluations in existing studies (Jiang et al., 2022; Luojus et al., 2021). Accordingly, these two products are derived from snow depth estimation based on passive microwave remote sensing and a fixed snow density (CSWE of 0.18 g/cm^3 and GlobSnow SWE of 0.24 g/cm^3). The corresponding snow depths of the two SWE products are acquired and then multiplied by STRF or ERA5-Land snow density to obtain optimized

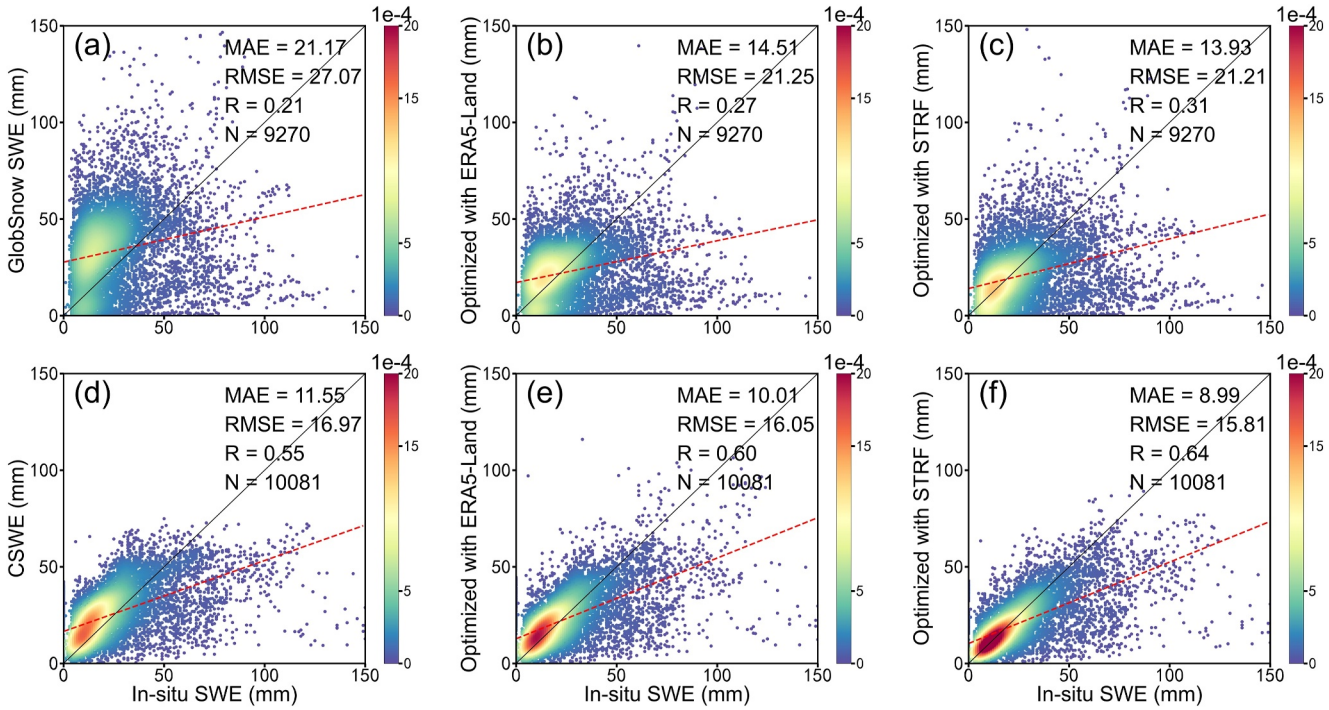

Figure 7. Accuracies of the original and optimized SWE products over China. (a) Original GlobSnow SWE, (b) optimized GlobSnow SWE with ERA5-Land snow density, (c) optimized GlobSnow SWE with STRF snow density, (d) original CSWE, (e) optimized CSWE with ERA5-Land snow density, and (f) optimized CSWE with STRF snow density.

SWE. In particular, STRF snow density based on temporal block cross-validation is used to further certify the temporal prediction ability of STRF model.

The accuracies of original and optimized SWE products are summarized in Figure 7, based on in-situ SWE observations. The optimized SWE with STRF snow density achieves the best accuracy, as the overestimation of GlobSnow SWE is obviously reduced and the R is increased from 0.21 to 0.31, the R of CSWE is increased from 0.55 to 0.64 and data are more concentrated on the 1:1 line. Although ERA5-Land snow density presents relative low accuracy (Figure 4), it still makes marginal contribution to improving SWE, revealing that using a constant snow density would undermine the accuracy of SWE and further demonstrating the importance of mapping the spatiotemporal distribution of snow density.

3.2. Snow Density Mapping

We produced the daily snow density data for snow-covered areas in China from 1980 to 2018 by applying the STRF model to gridded covariates, which is further masked by the AVHRR SCE data and CSWE to focus on snow pixels (Hao et al., 2021; Jiang et al., 2022). The data set is openly available in China Qinghai Tibet Plateau Scientific Data Center. (https://data.tpdc.ac.cn/zh-hans/data/81b5030e-828c-4271-baa7-66729b7ff1ae).

3.2.1. Spatiotemporal Distribution of Snow Density

The mean values of multiyear snow density are calculated for the entire snow season and different snow periods to assess the spatiotemporal distribution of snow density in stable snow cover areas in China, as shown in Figure 8. The average annual snow density shows that the QTP has the highest snow density above 0.162 g/cm^3, followed by XJ above 0.158 g/cm^3.

In the whole snow season (Figure 8a), the areas with high snow density are generally distributed in mountainous areas and northern QTP. During snow accumulation period (Figure 8b), three snow cover areas have an average snow density of 0.157 g/cm^3, with the average snow density in NIM being significantly lower than that in the other two areas. This could be because the deeper snow depth with higher overlying snow mass pressure and

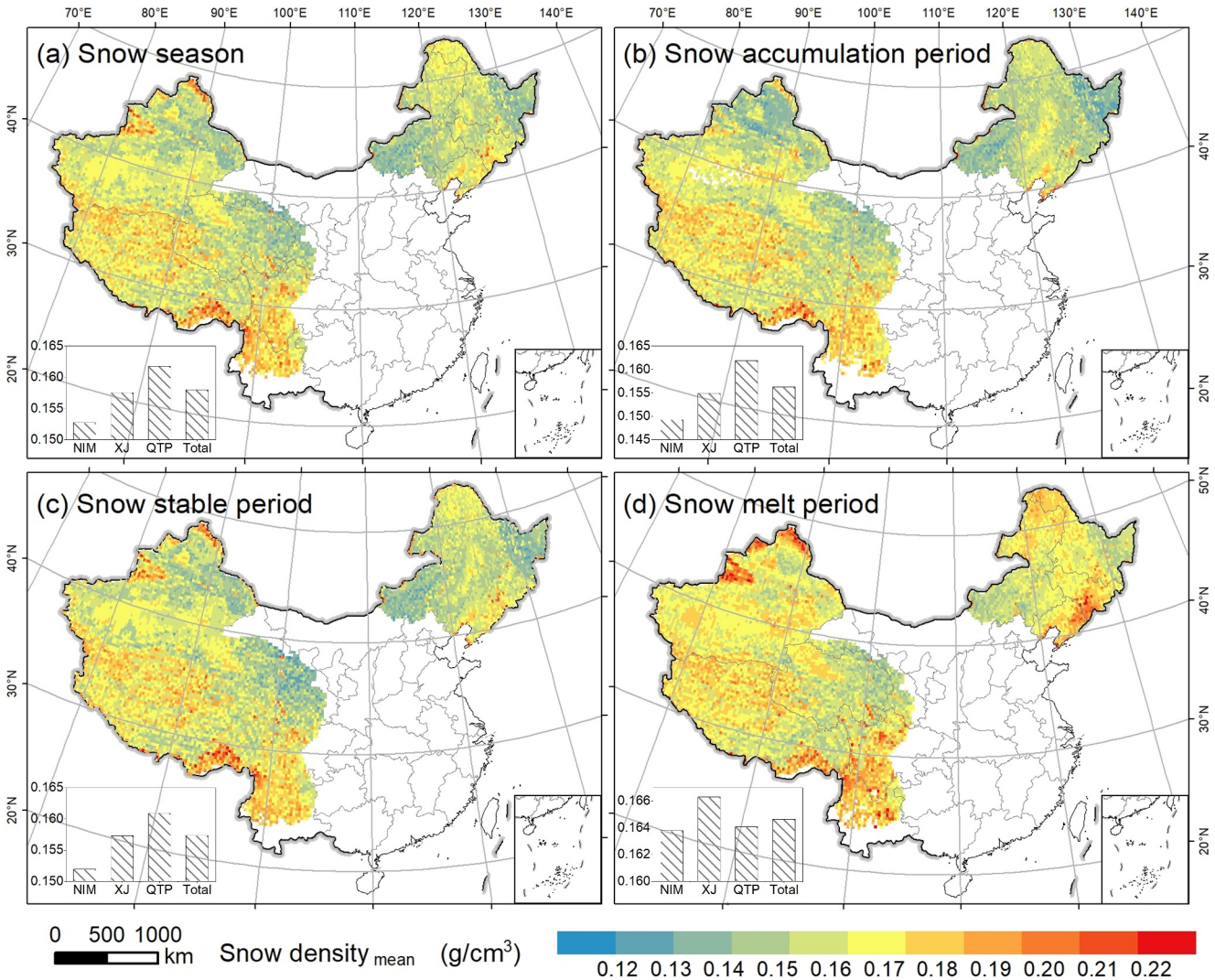

Figure 8. Spatiotemporal distribution of the mean annual snow density in entire snow season and different snow periods.

higher wind pressure and thus the larger snow density in XJ and mountains of QTP (Yang, Jiang & Lemmetyinen et al., 2020; Yang, Jiang & Luojus et al., 2020). In snow stable period (Figure 8c) with suitable temperature conditions for snow storage, the average snow density increases to 0.157 g/cm^3, particularly in mountainous areas where the highest snow density exceeds 0.18 g/cm^3. After entering snow melting period (Figure 8d) with sufficient spring water vapor and low temperature favoring snow melting and refreezing, the average snow density increases to 0.165 g/cm^3, particularly in XJ.

3.2.2. Temporal Change in Snow Density

The annual changing trends for the snow season and different snow periods are calculated in Figure 9 using the Mann–Kendall trend test. Additionally, the monthly changes in different snow cover areas are calculated to reflect temporal change of snow density within a year, as shown in Figure 11. The monthly or yearly average snow density are derived by exclusively considering snow-pixels while disregarding non-snow pixels, ensuring minimal impact on the results.

Overall, the annual snow density in snow season and different periods mainly show significant decreasing trends, especially in northern NIM and eastern QTP (Figure 9). Snow depth significantly changes snow density through gravity compaction. The annual snow depth of China from 1980 to 2018 shows a slightly decreasing trends (Jiang

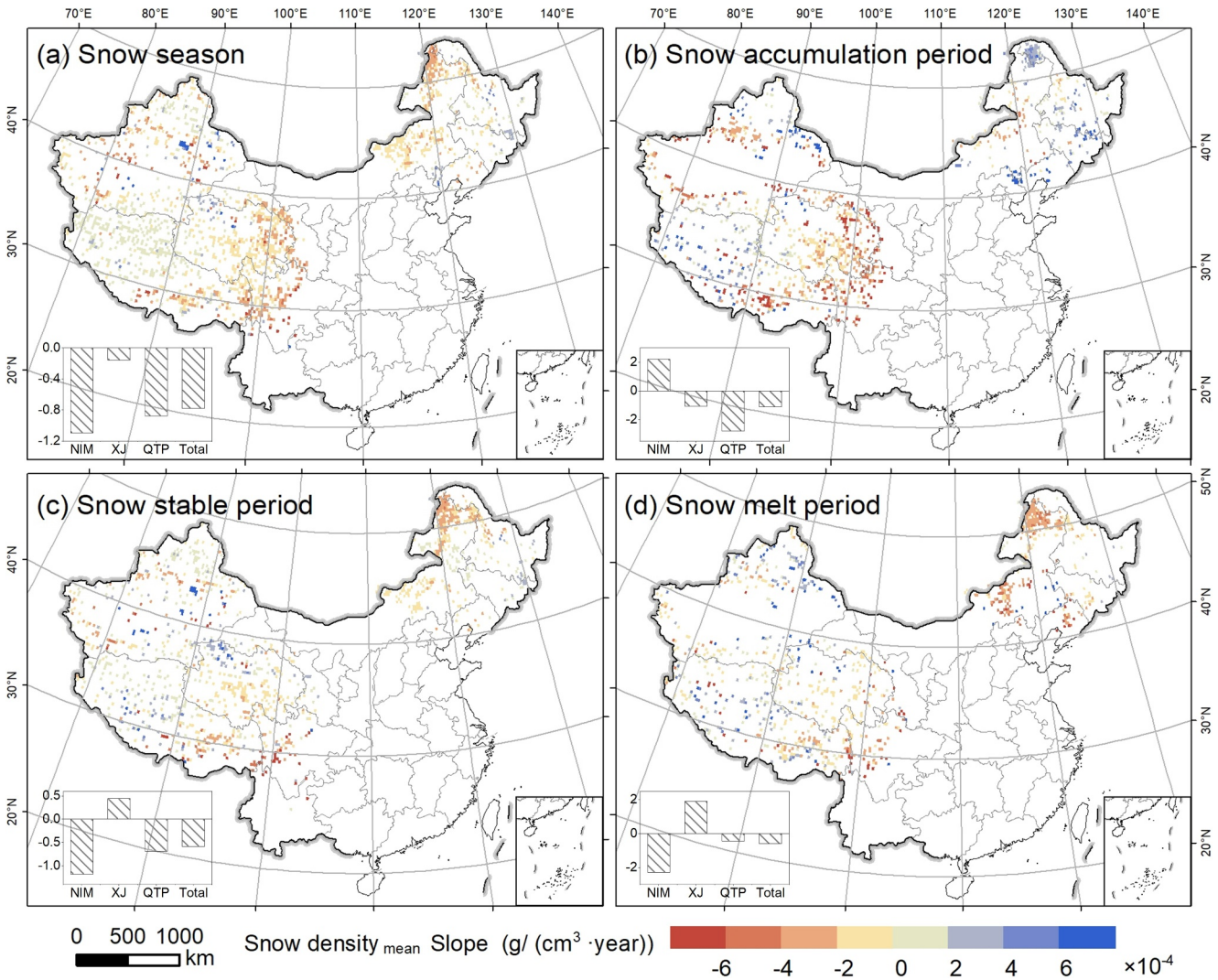

Figure 9. Spatial distribution of multiyear average snow density changing trends based on the Mann–Kendall trend test, with a significance level exceeding 95%.

et al., 2022), which is in line with our result of decreasing snow density. In the entire snow season (Figure 9a), the annual snow density gradually decreases with a slope of −0.778 g/(cm^3 year) ×10^{-4} and mostly appears in NIM with a slope of −1.09 g/(cm^3 year) ×10^{-4}. In contrast, the snow density shows an average increasing trend in NIM but an average decreasing trend in XJ and QTP in the snow accumulation period (Figure 9b). The change trend of annual snow density remains decreasing except for XJ during snow stable and melt periods (Figures 9c and 9d).

We further analyze the annual ERA5-Land snow density changing trends in snow season and different periods to reveal the reliability of STRF snow density changing trends (Figure 10). The ERA5-Land snow density mainly shows a significant decreasing trend from 1980 to 2018, which is consistent with STRF snow density. The difference is that ERA5 shows a significantly larger downward trend than the STRF trend, especially in the snow melt period (Figure 10d). Considering that ERA5-Land underestimate snow density over time (Gao, Li, Zhang & Chen et al., 2022; Gao, Li, Zhang & Zeng et al., 2022), STRF snow density with a decrease slope of −0.778 g/(cm^3 year) ×10^{-4} appears more reliable than ERA5-Land with a decrease slope of −1.330 g/(cm^3 year) ×10^{-4}.

At monthly scale, the change in snow density decreases from Sep. to the valley point in Dec. and then increases until May in the next year (Figure 11). The snow density decreases in snow accumulation period, which may be mainly attributed to frequent input of new snowfalls over the top of snowpacks with a very low snow density of approximately 0.05 g/cm^3 and partly attributed to deep frost development. With the snow accumulation, the temperature of lowest snow layer is higher than that of upper layer and these temperature gradient leads to

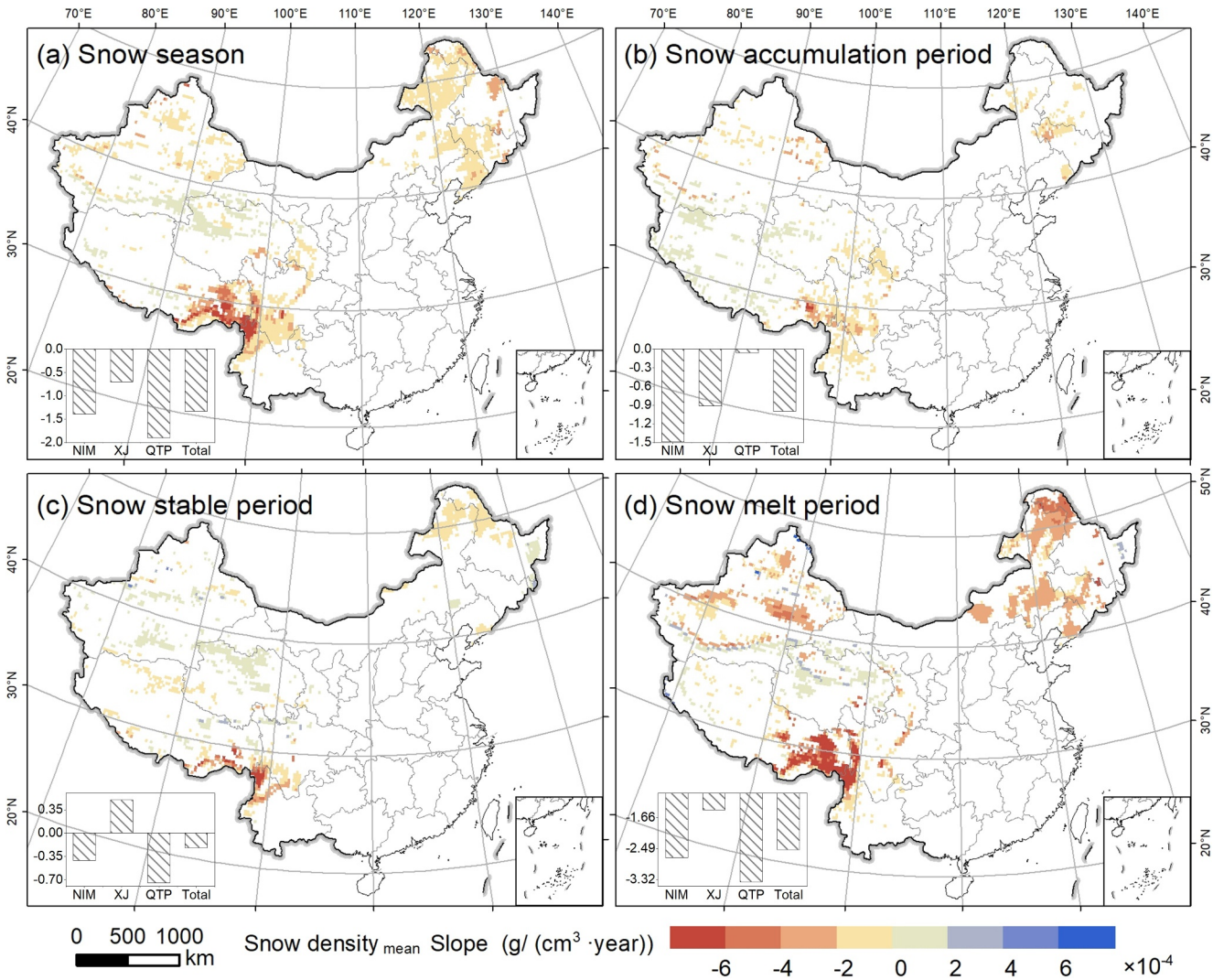

Figure 10. Spatial distribution of multiyear average ERA5-Land snow density changing trends based on the Mann–Kendall trend test, with a significance level exceeding 95%.

sintering phenomenon, finally forming deep frost and decreasing snow density (Seppälä, 1990). During snow stable periods, snow density rises due to the compaction and densification of snow. During the prophase of snow melt period, snow depth decreases with snow melts, and snow density gradually increases due to meltwater percolation (Colombo et al., 2023).

4. Discussion

Long-term and vast-scale snow density data are desperately needed for hydrological research and water management. However, ground measurements and remote sensing inversion are limited to large-scale snow density mapping (Elder et al., 1998; Gao, Li, Zhang & Chen et al., 2022; Gao, Li, Zhang & Zeng et al., 2022; Sturm et al., 2010), while physical models are governed by atmospheric forcing and statistical models, which may lack some modules to exactly match the measurements (Mizukami & Perica, 2008). The spatiotemporal dependent structure embedded in snow density is derived from spatiotemporal heterogeneity of snow density and nonlinear relations with covariates, being hardly interpreted by linear models. The proposed STRF model not only absorbs spatiotemporal covariates capable of depicting spatiotemporal dependent structure inherent in snow density, but also has the ability to handle nonlinear relations and extrapolate spatiotemporally, conducive to constructing accurate snow density, as proven by validations (see Figures 4–7).

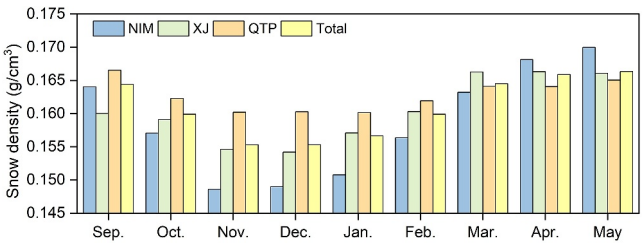

Figure 11. The monthly average snow density in different snow cover areas.

It is noted that the GTWNN model depending on parametric model structure could also depict the spatiotemporal dependent structure inherent in snow density and fit in-situ snow density, which shows great interpolation ability because of the inputting of snow density observation data (Wang et al., 2023). Considering the limited observation conditions, the GTWNN model are not able to obtain snow density maps outside these years. Accordingly, to derive long-term snow density across China, the STRF model is proposed to estimate snow density out range of in-situ series in the past periods. Apart from the essential difference, the STRF model integrates stronger ensemble learning model RF and more diverse covariates, providing environmental features for the nonlinear relations and particular spatiotemporal features for spatiotemporal heterogeneity of snow density, respectively. Although STRF does not have the assistance of inputting of in-situ snow density in inferencing procedure, it also achieves comparable accuracy (R^2 = 0.642) compared with GTWNN model (R^2 = 0.531) (Wang et al., 2023). More importantly, considering the essential differences between STRF and GTWNN, the STRF method can obtain long-term snow density data under limited observation conditions.

It has been agreed that the relations between snow density and covariates are weak-correlated and vary in different time and space (López-Moreno et al., 2013; Wang et al., 2023), posing great challenge to estimation but well overcome by STRF model. The feature importance analysis (Figure 3) highlights the effectiveness of snow-related and spatial covariates. We further compare the accuracies of models with different inputting data to analyze the advantage of embedded covariates, as shown in Table 2. Generally, the accuracy reaches the best when all features are involved, indicating that all the covariates play critical roles in model, especially for snow-related and geo-space features (Table 3). After adding the snow-related features, the R^2 increased by 25.4%, demonstrating the effectiveness of considering the snow process. As for Geo-space features, the invitation of expression of spatial heterogeneity increases R^2 from 0.561 to 0.642.

Although the proposed STRF model presents outstanding performance, there are still uncertainties in the STRF model, mainly coming from the data source and the RF structure. Observation error and uneven distribution of stations both lead to the problem of a lack of station representation. Remote sensing and reanalysis data are usually accompanied by structural errors, that is, pressure data with an R^2 of only about 0.4 (He et al., 2020). Although the RF model is powerful, it has apparent deficiencies from the demand of sufficient and balanced data, as reflected in the analysis of model accuracy at different spatiotemporal scales. The number and characteristics of samples vary in areas and thus bring about different learning performances of model, that is, 8,596 samples in NIM area and 942 samples in QTP. The biggest problem of machine learning model is that it relies on existing measurements, instead of physical laws. The model may be quite different in places not covered by in-situ sites, such as mountains with rare snow density measurements.

In the future, more long-term observation stations should be incorporated to enable the model to fully learn the temporal characteristics of snow density. Additionally, downscaling algorithms could be considered to increase the spatiotemporal resolution of snow density products, together with the utilization of stronger machine learning models, gradually improving the practicality and accuracy of snow density estimation.

5. Conclusions

The STRF model was proposed to map long-term and large-scale snow density in favor of in-situ measurements, multisource remote sensing, and reanalysis data. The superiority of STRF model comes from diverse covariates for addressing the spatiotemporal dependent structure inherent in snow density and strong learning model RF for handling nonlinear and weak-correlated relations between snow density and its

Table 3
Model Accuracies With Different Input Features, Where w/o Means Without Inputting the Feature Into the Model

Features	All	w/o snow-related	w/o meteorology	w/o vegetation	w/o time	w/o geo-space
MAE	0.024	0.029	0.023	0.024	0.024	0.027
RMSE	0.036	0.044	0.037	0.037	0.037	0.039
R^2	0.642	0.479	0.634	0.626	0.630	0.561

influencing factors. The embedded covariates are demonstrated to be conducive to snow density estimation, especially the snow-related and geo-space covariates with collective importance of 35.8% and 32.7%, emphasizing the magnitude of depicting snow evolution process and capturing spatial heterogeneity of snow density. Based on random and temporal block cross-validation against in-situ data, the STRF model achieves R^2 of 0.642, 0.326, MAEs of 0.024, 0.034 g/cm^3, and RMSEs of 0.036, 0.050 g/cm^3, exceeding ERA5-Land snow density. The STRF model performance is also validated by the spatial block cross-validation and independent validation. In addition, the optimization with dynamic STRF snow density improves the accuracies of CSWE and GlobSnow, increasing R from 0.55, 0.21 to 0.64, 0.31, respectively. With the benefit of STRF model, a data set of daily 25-km snow density from 1980 to 2018 in stable snow cover areas of China is produced, supporting us in obtaining the spatiotemporal patterns of snow density and probably assisting in water resource management.

Data Availability Statement

Our research primarily utilizes three types of data: in-situ data, remote sensing data, and reanalysis data. Daily measurements of snow depth and snow pressure are obtained from the China Meteorological Administration (CMA), which should be authorized to redistribute. The remote sensing and reanalysis data utilized in our study are sourced from open-access platforms. These include the Advanced Very High Resolution Radiometer (AVHRR) SCE data (https://doi.org/10.11888/Snow.tpdc.271381), the passive microware remote sensing snow depth data (http://www.doi.org/10.11922/sciencedb.j00076.00071), China Regional Surface Meteorological Element Driven Data set (https://doi.org/10.6084/m9.figshare.c.4557599.v1), the Shuttle Radar Topography Mission digital elevation model (http://www.dsac.cn/DataP), and the ECMWF ERA5-Land hourly data set (https://cds.climate.copernicus.eu).

Acknowledgments
This study is supported by the National Natural Science Foundation of China (Grant number 42171307), the AI & AI for Science Project of Nanjing University, the "GeoX" Interdisciplinary Research Funds for the Frontiers Science Center for Critical Earth Material Cycling, Nanjing University, and the Fundamental Research Funds for the Central Universities (Grant number 020914380119).

References

Anderton, S. P., White, S. M., & Alvera, B. (2004). Evaluation of spatial variability in snow water equivalent for a high mountain catchment. *Hydrological Processes*, *18*(3), 435–453. https://doi.org/10.1002/hyp.1319

Bonner, H. M., Raleigh, M. S., & Small, E. E. (2022). Isolating forest process effects on modelled snowpack density and snow water equivalent. *Hydrological Processes*, *36*(1), e14475. https://doi.org/10.1002/hyp.14475

Bormann, K. J., Westra, S., Evans, J. P., & McCabe, M. F. (2013). Spatial and temporal variability in seasonal snow density. *Journal of Hydrology*, *484*, 63–73. https://doi.org/10.1016/j.jhydrol.2013.01.032

Breiman, L. (2001). Random forests. *Machine Learning*, *45*(1), 5–32. https://doi.org/10.1023/a:1010933404324

Broxton, P. D., Leeuwen, W. J. D., & Biederman, J. A. (2019). Improving snow water equivalent maps with machine learning of snow survey and Lidar measurements. *Water Resources Research*, *55*(5), 3739–3757. https://doi.org/10.1029/2018WR024146

Bruland, O., Færevåg, Å., Steinsland, I., Liston, G. E., & Sand, K. (2015). Weather SDM: Estimating snow density with high precision using snow depth and local climate. *Hydrology Research*, *46*(4), 494–506. https://doi.org/10.2166/nh.2015.059

Che, T., Dai, L., Zheng, X., Li, X., & Zhao, K. (2016). Estimation of snow depth from passive microwave brightness temperature data in forest regions of northeast China. *Remote Sensing of Environment*, *183*, 334–349. https://doi.org/10.1016/j.rse.2016.06.005

Clark, M. P., Hendrikx, J., Slater, A. G., Kavetski, D., Anderson, B., Cullen, N. J., et al. (2011). Representing spatial variability of snow water equivalent in hydrologic and land-surface models: A review: Representing spatial variability of SWE in models. *Water Resources Research*, *47*(7). https://doi.org/10.1029/2011WR010745

Colombo, R., Pennati, G., Pozzi, G., Garzonio, R., Di Mauro, B., Giardino, C., et al. (2023). Mapping snow density through thermal inertia observations. *Remote Sensing of Environment*, *284*, 113323. https://doi.org/10.1016/j.rse.2022.113323

Dai, L., & Che, T. (2011). Spatiotemporal distributions and influences on snow density in China from 1999 to 2008. *Sciences in Cold and Arid Regions*, *3*(4), 0325–0331. https://doi.org/10.3724/SP.J.1226.2011.00325

Dai, L., Che, T., Xie, H., & Wu, X. (2018). Estimation of snow depth over the Qinghai-Tibetan plateau based on AMSR-E and MODIS data. *Remote Sensing*, *10*(12), 1989. https://doi.org/10.3390/rs10121989

Durand, Y., Giraud, G., Brun, E., Mérindol, L., & Martin, E. (1999). A computer-based system simulating snowpack structures as a tool for regional avalanche forecasting. *Journal of Glaciology*, *45*(151), 469–484. https://doi.org/10.3189/S0022143000001337

Elder, K., Rosenthal, W., & Davis, R. E. (1998). Estimating the spatial distribution of snow water equivalence in a montane watershed. *Hydrological Processes*, *12*(10–11), 1793–1808. https://doi.org/10.1002/(SICI)1099-1085(199808/09)12:10/11<1793::AID-HYP695>3.0.CO;2-K

Essery, R., Pomeroy, J., Ellis, C., & Link, T. (2008). Modelling longwave radiation to snow beneath forest canopies using hemispherical photography or linear regression. *Hydrological Processes*, *22*(15), 2788–2800. https://doi.org/10.1002/hyp.6930

Fontrodona-Bach, A., Schaefli, B., Woods, R., Teuling, A. J., & Larsen, J. R. (2023). NH-SWE: Northern Hemisphere Snow Water Equivalent dataset based on in situ snow depth time series. *Earth System Science Data*, *15*(6), 2577–2599. https://doi.org/10.5194/essd-15-2577-2023

Gao, S., Li, Z., Zhang, P., Chen, Q., Zeng, J., Zhao, C., et al. (2022b). Global sensitivity analysis of the MEMLS model for retrieving snow water equivalent. *IEEE Transactions on Geoscience and Remote Sensing*, *60*, 1–15. https://doi.org/10.1109/TGRS.2021.3134695

Gao, S., Li, Z., Zhang, P., Zeng, J., Chen, Q., Zhao, C., et al. (2022a). An assessment of the applicability of three reanalysis snow density datasets over China using ground observations. *IEEE Geoscience and Remote Sensing Letters*, *19*, 1–5. https://doi.org/10.1109/LGRS.2022.3202897

Gao, X., Pan, J., Peng, Z., Zhao, T., Bai, Y., Yang, J., et al. (2023). Snow density retrieval in Quebec using space-borne SMOS observations. *Remote Sensing*, *15*(8), 2065. https://doi.org/10.3390/rs15082065

Goovaerts, P. (1997). Geostatistics for natural resources evaluation. In *Applied Geostatistics Series*. Oxford University Press, Cambridge University Press. https://doi.org/10.1017/S0016756898631502

Grünewald, T., Schirmer, M., Mott, R., & Lehning, M. (2010). Spatial and temporal variability of snow depth and ablation rates in a small mountain catchment. *The Cryosphere*, *4*(2), 215–225. https://doi.org/10.5194/tc-4-215-2010

Hao, X., Huang, G., Che, T., Ji, W., Sun, X., Zhao, Q., et al. (2021). The NIEER AVHRR snow cover extent product over China – A long-term daily snow record for regional climate research. *Earth System Science Data*, *13*(10), 4711–4726. https://doi.org/10.5194/essd-13-4711-2021

He, J., Yang, K., Tang, W., Lu, H., Qin, J., Chen, Y., & Li, X. (2020). The first high-resolution meteorological forcing dataset for land process studies over China. *Scientific Data*, *7*(1), 25. https://doi.org/10.1038/s41597-020-0369-y

Hu, Y., Che, T., Dai, L., & Xiao, L. (2021). Snow depth fusion based on machine learning methods for the northern hemisphere. *Remote Sensing*, *13*(7), 1250. https://doi.org/10.3390/rs13071250

Huang, X., Deng, J., Ma, X., Wang, Y., Feng, Q., Hao, X., & Liang, T. (2016). Spatiotemporal dynamics of snow cover based on multi-source remote sensing data in China. *The Cryosphere*, *10*(5), 2453–2463. https://doi.org/10.5194/tc-10-2453-2016

Huang, X., Liu, C., Wang, Y., Feng, Q., & Liang, T. (2019). Snow cover variations across China from 1952–2012 (preprint). *Snow/Seasonal Snow*. https://doi.org/10.5194/tc-2019-152

Jiang, L., Yang, J., Zhang, C., Wu, S., Li, Z., Dai, L., et al. (2022). Daily snow water equivalent product with SMMR, SSM/I and SSMIS from 1980 to 2020 over China. *Big Earth Data*, *6*(4), 1–15. https://doi.org/10.1080/20964471.2022.2032998

Jonas, T., Marty, C., & Magnusson, J. (2009). Estimating the snow water equivalent from snow depth measurements in the Swiss Alps. *Journal of Hydrology*, *378*(1–2), 161–167. https://doi.org/10.1016/j.jhydrol.2009.09.021

Ke, C., Li, X., Xie, H., Ma, D., Liu, X., & Kou, C. (2016). Variability in snow cover phenology in China from 1952 to 2010. *Hydrology and Earth System Sciences*, *20*(2), 755–770. https://doi.org/10.5194/hess20-755-2016

Lehning, M., Bartelt, P., Brown, B., Fierz, C., & Satyawali, P. (2002). A physical SNOWPACK model for the Swiss avalanche warning Part II. Snow microstructure. *Cold Regions Science and Technology*, *35*(3), 169–184. https://doi.org/10.1016/s0165-232x(02)00072-1

Li, M., Xiao, P., Zhang, X., Feng, X., & Zhu, L. (2022). An improved approach of dry snow density estimation using C-band synthetic aperture radar data. *ISPRS Journal of Photogrammetry and Remote Sensing*, *191*, 49–67. https://doi.org/10.1016/j.isprsjprs.2022.07.002

López-Moreno, J. I., Fassnacht, S. R., Heath, J. T., Musselman, K. N., Revuelto, J., Latron, J., et al. (2013). Small scale spatial variability of snow density and depth over complex alpine terrain: Implications for estimating snow water equivalent. *Advances in Water Resources*, *55*, 40–52. https://doi.org/10.1016/j.advwatres.2012.08.010

Luojus, K., Pulliainen, J., Takala, M., Lemmetyinen, J., Mortimer, C., Derksen, C., et al. (2021). GlobSnow v3.0 Northern Hemisphere snow water equivalent dataset. *Scientific Data*, *8*(1), 163. https://doi.org/10.1038/s41597-021-00939-2

McCreight, J. L., & Small, E. E. (2014). Modeling bulk density and snow water equivalent using daily snow depth observations. *The Cryosphere*, *8*(2), 521–536. https://doi.org/10.5194/tc-8-521-2014

Meloche, J., Langlois, A., Rutter, N., McLennan, D., Royer, A., Billecocq, P., & Ponomarenko, S. (2022). High-resolution snow depth prediction using random forest algorithm with topographic parameters: A case study in the Greiner watershed, Nunavut. *Hydrological Processes*, *36*(3). https://doi.org/10.1002/hyp.14546

Mizukami, N., & Perica, S. (2008). Spatiotemporal characteristics of snowpack density in the mountainous regions of the western United States. *Journal of Hydrometeorology*, *9*(6), 1416–1426. https://doi.org/10.1175/2008JHM981.1

Muñoz-Sabater, J., Dutra, E., Agustí-Panareda, A., Albergel, C., Arduini, G., Balsamo, G., et al. (2021). ERA5-Land: A state-of-the-art global reanalysis dataset for land applications. *Earth System Science Data*, *13*(9), 4349–4383. https://doi.org/10.5194/essd-13-4349-2021

Prasad, A. M., Iverson, L. R., & Liaw, A. (2006). Newer classification and regression tree techniques: Bagging and random forests for ecological prediction. *Ecosystems*, *9*(2), 181–199. https://doi.org/10.1007/s10021-005-0054-1

Pu, Z., & Xu, L. (2009). MODIS/Terra observed snow cover over the Tibet plateau: Distribution, variation and possible connection with the East Asian summer monsoon (EASM). *Theoretical and Applied Climatology*, *97*(3–4), 265–278. https://doi.org/10.1007/s00704-008-0074-9

Pu, Z., Xu, L., & Salomonson, V. V. (2007). MODIS/Terra observed seasonal variations of snow cover over the Tibetan Plateau. *Geophysical Research Letters*, *34*(6), L06706. https://doi.org/10.1029/2007GL029262

Raleigh, M. S., & Small, E. E. (2017). Snowpack density modeling is the primary source of uncertainty when mapping basin-wide SWE with Lidar. *Geophysical Research Letters*, *44*(8), 3700–3709. https://doi.org/10.1002/2016GL071999

Ran, Y. H., Li, X., Lu, L., & Li, Z. Y. (2012). Large-scale land cover mapping with the integration of multi-source information based on the Dempster–Shafer theory. *International Journal of Geographical Information Science*, *26*(1), 169–191. https://doi.org/10.1080/13658816.2011.577745

Revuelto, J., López-Moreno, J. I., Azorin-Molina, C., & Vicente-Serrano, S. M. (2014). Topographic control of snowpack distribution in a small catchment in the central Spanish Pyrenees: Intra- and inter-annual persistence. *The Cryosphere*, *8*(5), 1989–2006. https://doi.org/10.5194/tc-8-1989-2014

Roberts, D. R., Bahn, V., Ciuti, S., Boyce, M. S., Elith, J., Guillera-Arroita, G., et al. (2017). Cross-validation strategies for data with temporal, spatial, hierarchical, or phylogenetic structure. *Ecography*, *40*(8), 913–929. https://doi.org/10.1111/ecog.02881

Rodriguez, J. D., Perez, A., & Lozano, J. A. (2010). Sensitivity analysis of K-fold cross validation in prediction error estimation. *IEEE Transactions on Pattern Analysis and Machine Intelligence*, *32*(3), 569–575. https://doi.org/10.1109/TPAMI.2009.187

Seppälä, M. (1990). Depth of snow and frost on a Palsa Mire, Finnish Lapland. *Geografiska Annaler - Series A: Physical Geography*, *72*(2), 191–201. https://doi.org/10.1080/04353676.1990.11880315

Shepard, D. (1968). A two-dimensional interpolation function for irregularly-spaced data. In *Proceedings of the 1968 23rd ACM National Conference* (pp. 517–524). ACM Press. https://doi.org/10.1145/800186.810616

Stock, A. (2022). Spatiotemporal distribution of labeled data can bias the validation and selection of supervised learning algorithms: A marine remote sensing example. *ISPRS Journal of Photogrammetry and Remote Sensing*, *187*, 46–60. https://doi.org/10.1016/j.isprsjprs.2022.02.023

Storck, P., Lettenmaier, D. P., & Bolton, S. M. (2002). Measurement of snow interception and canopy effects on snow accumulation and melt in a mountainous maritime climate, Oregon, United States: Forest canopy effects on ground snow pack dynamics. *Water Resources Research*, *38*(11), 5-1-5–16. https://doi.org/10.1029/2002WR001281

Sturm, M., Taras, B., Liston, G. E., Derksen, C., Jonas, T., & Lea, J. (2010). Estimating snow water equivalent using snow depth data and climate classes. *Journal of Hydrometeorology*, *11*(6), 1380–1394. https://doi.org/10.1175/2010JHM1202.1

Sturm, M., & Wagner, A. M. (2010). Using repeated patterns in snow distribution modeling: An Arctic example: Repeated snow patterns. *Water Resources Research*, *46*(12). https://doi.org/10.1029/2010WR009434

Svoma, B. M. (2011). Winter climatic controls on spring snowpack density in the western United States. *Arctic Antarctic and Alpine Research*, *43*(1), 118–126. https://doi.org/10.1657/1938-4246-43.1.118

Trujillo, E., Ramírez, J. A., & Elder, K. J. (2007). Topographic, meteorologic, and canopy controls on the scaling characteristics of the spatial distribution of snow depth fields: Spatial scaling of snow depth. *Water Resources Research*, *43*(7). https://doi.org/10.1029/2006WR005317

Valt, M., Guyennon, N., Salerno, F., Petrangeli, A. B., Salvatori, R., Cianfarra, P., & Romano, E. (2018). Predicting new snow density in the Italian Alps: A variability analysis based on 10 years of measurements. *Hydrological Processes*, *32*(20), 3174–3187. https://doi.org/10.1002/hyp.13249

Venäläinen, P., Luojus, K., Mortimer, C., Lemmetyinen, J., Pulliainen, J., Takala, M., et al. (2023). Implementing spatially and temporally varying snow densities into the GlobSnow snow water equivalent retrieval. *The Cryosphere*, *17*(2), 719–736. https://doi.org/10.5194/tc-17-719-2023

Wang, H., Zhang, X., Xiao, P., Che, T., Zheng, Z., Dai, L., & Luan, W. (2023). Towards large-scale daily snow density mapping with spatio-temporally aware model and multi-source data. *The Cryosphere*, *17*(1), 33–50. https://doi.org/10.5194/tc-17-33-2023

Wang, H., Zhang, X., Xiao, P., Zhang, K., & Wu, S. (2022). Elevation-dependent response of snow phenology to climate change from a remote sensing perspective: A case survey in the central Tianshan Mountains from 2000 to 2019. *International Journal of Climatology*, *42*(3), 1706–1722. https://doi.org/10.1002/joc.7330

Wetlaufer, K., Hendrikx, J., & Marshall, L. (2016). Spatial heterogeneity of snow density and its influence on snow water equivalence estimates in a large mountainous basin. *Hydrology*, *3*(1), 3. https://doi.org/10.3390/hydrology3010003

Winstral, A., & Marks, D. (2014). Long-term snow distribution observations in a mountain catchment: Assessing variability, time stability, and the representativeness of an index site: Long-term snow distribution observations. *Water Resources Research*, *50*(1), 293–305. https://doi.org/10.1002/2012WR013038

Yang, J., Jiang, L., Luojus, K., Pan, J., Lemmetyinen, J., Takala, M., & Wu, S. (2020). Snow depth estimation and historical data reconstruction over China based on a random forest machine learning approach. *The Cryosphere*, *14*(6), 1763–1778. https://doi.org/10.5194/tc-14-1763-2020

Yang, J., Jiang, L., Wu, S., Wang, G., Wang, J., & Liu, X. (2019). Development of a snow depth estimation algorithm over China for the FY-3D/MWRI. *Remote Sensing*, *11*(8), 977. https://doi.org/10.3390/rs11080977

Yang, J. W., Jiang, L. M., Lemmetyinen, J., Luojus, K., Takala, M., Wu, S. L., & Pan, J. M. (2020). Validation of remotely sensed estimates of snow water equivalent using multiple reference datasets from the middle and high latitudes of China. *Journal of Hydrology*, *590*, 125499. https://doi.org/10.1016/j.jhydrol.2020.125499

Zaremehrjardy, M., Razavi, S., & Faramarzi, M. (2021). Assessment of the cascade of uncertainty in future snow depth projections across watersheds of mountainous, foothill, and plain areas in northern latitudes. *Journal of Hydrology*, *598*, 125735. https://doi.org/10.1016/j.jhydrol.2020.125735

Zhang, J., Pohjola, V. A., Pettersson, R., Norell, B., Marchand, W.-D., Clemenzi, I., & Gustafsson, D. (2021). Improving the snowpack monitoring in the mountainous areas of Sweden from space: A machine learning approach. *Environmental Research Letters*, *16*(8), 084007. https://doi.org/10.1088/1748-9326/abfe8d

Zhong, X., Zhang, T., Kang, S., & Wang, J. (2021). Spatiotemporal variability of snow cover timing and duration over the Eurasian continent during 1966–2012. *Science of the Total Environment*, *750*, 141670. https://doi.org/10.1016/j.scitotenv.2020.141670

Zhong, X., Zhang, T., & Wang, K. (2014). Snow density climatology across the former USSR. *The Cryosphere*, *8*(2), 785–799. https://doi.org/10.5194/tc-8-785-2014